

Article

Catalytic Combustion of Diesel Soot on Ce/Zr Series Catalysts Prepared by Sol-Gel Method

Chaoqian Ai ^{1,2}, Yaoyao Zhang ², Pan Wang ³ and Wei Wang ^{1,2,*} 

¹ Department of Chemical Engineering, College of Environment Science and Engineering, Chang'an University, Xi'an 710054, China

² Key Laboratory of Subsurface Hydrology and Ecology in Arid Areas, Ministry of Education Chang'an University, Xi'an 710054, China

³ School of Automotive and Traffic Engineering, Jiangsu University, Zhenjiang 212013, China

* Correspondence: wwchem@126.com; Tel.: +86-1357-242-9632

Received: 1 July 2019; Accepted: 26 July 2019; Published: 29 July 2019



Abstract: Cerium-zirconium (Ce-Zr) solid solutions have been extensively used in a wide variety of catalytic processes due to their unique catalytic features in conjunction with lower cost compared to noble metal-based systems. A series of Ce-Zr-based catalysts was prepared by the sol-gel method. The structure and morphology of these catalysts were characterized by X-ray diffraction, thermogravimetric-differential scanning calorimetry, scanning electron microscopy, energy dispersive spectroscopy, and X-ray photoelectron spectroscopy. Furthermore, investigation on catalytic performance was carried out by constructing a test platform, and the result indicated that the catalysts apparently decreased the soot ignition temperature. These catalysts exhibited higher catalytic activity for soot oxidation under narrow contact conditions. The results revealed that some soot particles could react with adsorbed oxygen, and other part of diesel soot reacted with lattice oxygen. The activity of these catalysts was attributed to synergistic effect arising from the combination of K/Co/Zr and Ce-Zr solid solution, which led to the decrease in the ignition temperature to 294 °C (data from the test platform). The catalyst still keeps good stability and catalytic activity after the cycle oxidation experiment. A reaction pathway was proposed to explain catalytic combustion process of soot, i.e., combination of K/Co/Zr with Ce-Zr solid solution reduced the binding energy of Ce-Zr solid solution, which was conducive to provide more active sites to release the active oxygen (O₂⁻) or lattice oxygen (O²⁻).

Keywords: cerium-zirconium solid solution; ignition temperature; soot combustion; catalytic activity

1. Introduction

Nowadays, humanity is facing various environmental problems, such as water pollution and air pollution, and a great number of researchers have reported different ways to treat contaminants [1–4]. Among them, the problem of air pollution is particularly prominent. Owing to the negative and hazardous environmental and health impacts of diesel particulate matter (PM) [5–8] and the necessity of complying with increasingly stringent automobile emissions regulations, significant research efforts to reduce PM emissions are ongoing, even though achievement of such reductions remains challenging [9]. PM is primarily composed of carbonaceous particles (also called soot), with diameters ranging from a few nanometers (10–20 nm) to several hundred nanometers [10]. These particles originate from incomplete in-cylinder oxidation of the fuel. Trapping of PM using a filter is an efficient way of eliminating this pollutant. In this approach, soot particles are separated from the gas phase by filtration through porous ceramic media. The particulates are accumulated in the channels of filter, pressure drop across the filter increases, and after some time, burning of soot particles accumulated inside

the filter becomes necessary. Soot burns at 500–600 °C under air conditions, while the diesel exhaust temperature is only 200–400 °C. Therefore, igniting soot combustion under these conditions requires catalytic oxidation. The filter should be able to trap and burn soot particles when it collects them, so that the filter does not saturate. A large number of catalysts has been investigated for controlling the exhaust emissions of diesel engines, and the main objective of most of these studies is to improve the catalytic performance for soot combustion. Numerous articles reporting the use of CeO₂ as an effective catalyst for soot combustion are available [11,12], and a mechanism has been proposed to explain these catalytic processes. The Ce⁴⁺/Ce³⁺ redox cycle confers the ability to absorb gaseous O₂, thus forming active oxygen at the catalyst surface (O_{ads}), which can be transferred to the soot catalyst interface by superficial diffusion. For this reason, properties of the Ce⁴⁺/Ce³⁺ couple and the capacity of CeO₂ to exchange oxygen with the gas phase make CeO₂-based materials one of the most promising catalysts for soot combustion [13,14].

They are widely known to favor the oxidation of soot by increasing the catalyst/soot contact with the high mobility of alkali metals or alkaline-earth metals [15–20]. Fan et al. studied the effect of Ba loading on Cu-Ce catalysts, and it was shown that Ba restrains the sintering of (Cu, Ce)O_x, resulting in relatively more favorable redox properties and thus higher activity for NO oxidation [20]. A great number of researchers also studied the effect of alkali metals loading in a catalyst. Aneghi's group pointed out that the order of activity in soot oxidation depends on the nature (Cs > Rb ≈ K > Na) and the amount of the metal [21]. Weng's study showed that the pronouncedly enhanced NO_x storage capacity by potassium modification were especially important in the NO_x-assisted soot oxidation reaction with the K/CuCe catalyst [22]. Shan pointed out that K has strong fluidity on the CeO₂, which is beneficial to the effective contact of the catalyst with carbon black [23].

Furthermore, it is an accepted idea that the doping of Zr, Hf, and rare-earth metals can enhance the oxygen storage capacity of Ce; however, their contribution toward soot oxidation is complex [24]. Aneghi et al. studied soot oxidation over Ce_xZr_{1-x}O₂ under different atmospheres, and found that the surface oxygen plays an important role in soot oxidation reactions in O₂-rich environments [25]. The Ce_xZr_{1-x}O₂ catalytic series exhibits excellent catalytic performance; however, the temperature corresponding to the maximum soot combustion rate (T_{max}) is still too high [26–28]. Jing X et al. studied spinel-type Pd_xCo_{3-x}O₄ binary active sites on 3D ordered meso-macroporous Ce-Zr-O₂ for catalytic soot oxidation. Pd²⁺ cations can be substitute for the A sites (Co²⁺ cations) in supported Co₃O₄ NPs with a spinel-type AB₂O₄ structure, and spinel-type Pd_xCo_{3-x}O₄ biactive sites enhance the activation efficiency for O₂ and NO reactants remarkably [29]. The synergistic effect between Pt and Ce_xZr_{1-x}O₂ may further improve the catalytic performance because Pt can accelerate the mobility of the active oxygen in Ce_xZr_{1-x}O₂ [30,31]. However, the precious metal Pt is very expensive and easily get inactivated in exhaust atmosphere. Therefore, it is still a huge challenge to develop highly efficient, and economical catalyst with long life period in soot combustion field. Doping metal oxides (such as K, Co) on Ce_xZr_{1-x}O₂ for catalytic soot oxidation has a great research value.

According to the oxide catalysts reported, the much cheaper CeO₂ stabilized with ZrO₂ as mixed oxide formulations Ce_xZr_{1-x}O₂ catalysts have evidenced high soot oxidation performance in O₂ atmosphere. In this study, Ce-Zr oxide solid solution catalysts (K/Zr_{0.84}Ce_{0.16}O₂, Zr/Zr_{0.84}Ce_{0.16}O₂, Co/Zr_{0.84}Ce_{0.16}O₂, Zr_{0.84}Ce_{0.16}O₂, Co/Ce_{0.75}Zr_{0.25}O₂ and Ce_{0.75}Zr_{0.25}O₂) were prepared by sol-gel method, and these catalysts were tested in a platform to explore the catalytic properties towards soot particles. The results revealed that some soot particles could react with adsorbed oxygen, and other part of diesel soot could react with lattice oxygen. The remarkable catalytic performance, thermostability, and repetition stability of catalysts make them potential candidates for diesel emission control. Furthermore, a reaction pathway was proposed for comprehensive understanding of the catalytic oxidation of diesel soot using the as-fabricated catalysts.

2. Results and Discussion

2.1. Synthesis and Structure of the Catalysts

2.1.1. Morphological Characterization of the Catalysts by Scanning Electron Microscopy

Figure 1a,c show SEM images of $\text{Ce}_{0.75}\text{Zr}_{0.25}\text{O}_2$ (CZ) and $\text{Zr}_{0.84}\text{Ce}_{0.16}\text{O}_2$ (ZC), clearly showing the aggregation of smaller particles to form a dense bigger particle in CZ and ZC samples. Cobalt-doped ZC (Co/ZC) forms thick flaky structure, as shown in Figure 1b. Compared to Figure 1a,c,e, ZC catalyst doped with K presents a different structure, which was more loose rather than dense, just as marked in red. Figure 1f present SEM images of Zr/ZC catalyst formed a layered structure. There are many small deposits presented on the large particles seen in Figure 1b,d. This means that small catalytic particles will achieve a closer contact with the soot, and we predict it may have a better catalytic performance.

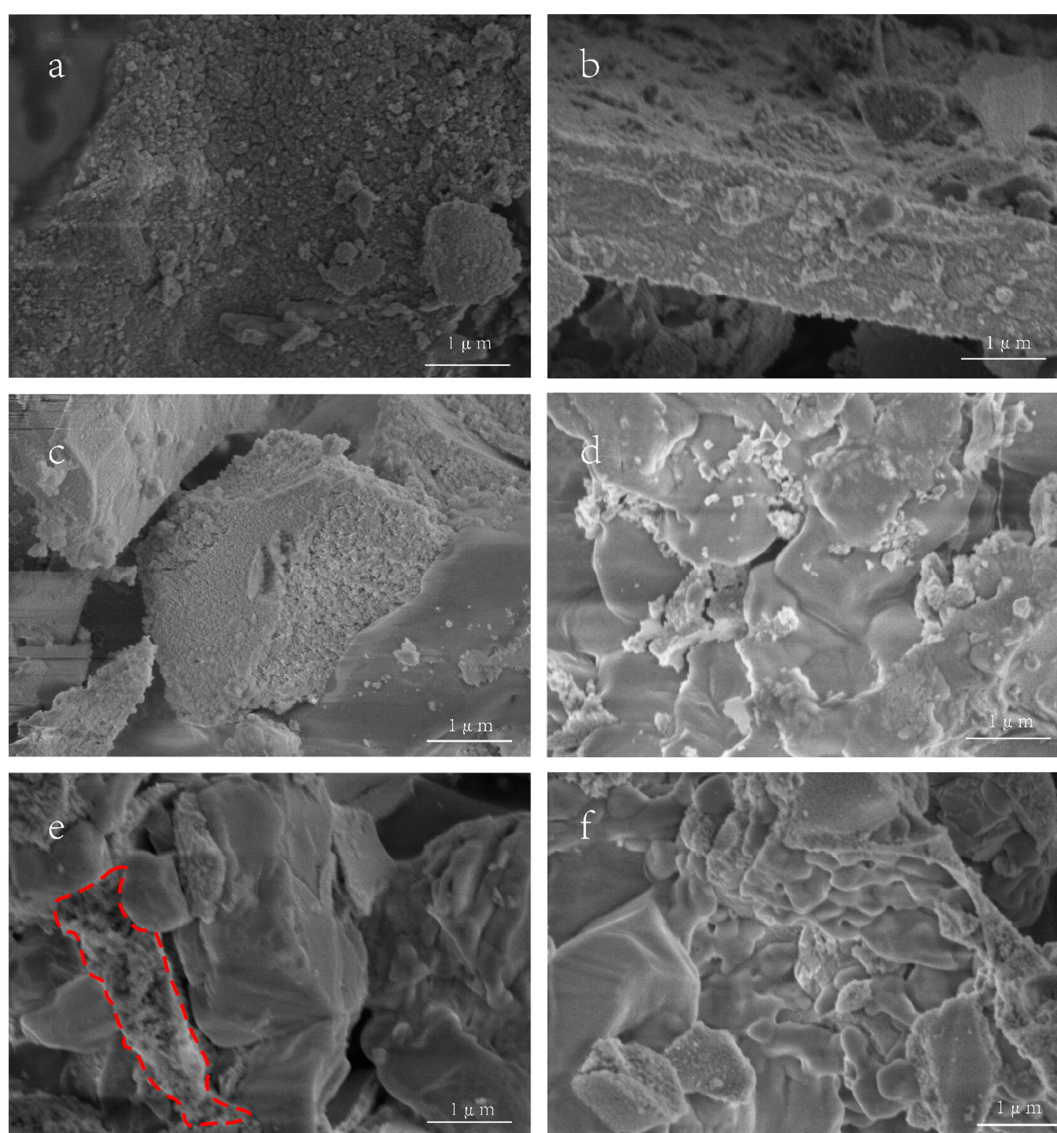


Figure 1. SEM morphologies of the catalysts (a) CZ, (b) Co/CZ, (c) ZC, (d) Co/ZC, (e) K/ZC, (f) Zr/ZC.

2.1.2. X-ray Diffraction Patterns of the Catalysts

XRD patterns of samples are shown in Figure 2. Peaks ascribed to CZ and ZC are detected in all samples, indicating that Ce-Zr solid solutions ($\text{Ce}_{0.75}\text{Zr}_{0.25}\text{O}_2$, $\text{Zr}_{0.84}\text{Ce}_{0.16}\text{O}_2$) are easily formed and these are the main phase compositions of products. Simultaneously, some peaks of metal oxides (ZrO_2 ,

Co_3O_4 , and K_2CeO_2) coexist in samples because of the introduction of excessive amount of chemical reagents in case of metal oxides doping. XRD patterns exhibit the characteristic diffraction peaks of ZrO_2 at 31.878° , 31.971° , and 34.209° (JCPDS No. 49-1746). The characteristic diffraction peaks of Co_3O_4 can be observed at 36.852° and 44.808° (JCPDS No. 44-1467). The characteristic diffraction peaks of K_2CeO_3 are observed at 34.480° and 49.554° (JCPDS No. 31-0989). The sol-gel method not only lowers the sintering temperature because it provides fine grains and homogeneous composition, but also makes the starting materials homogeneous according to the design stoichiometric ratio. One part of metal oxides was used to form CZ and ZC, and the other part of metal oxides was maintained in final product, in which coordination effect was caused on surface of catalysts to decrease the combustion temperature of soot.

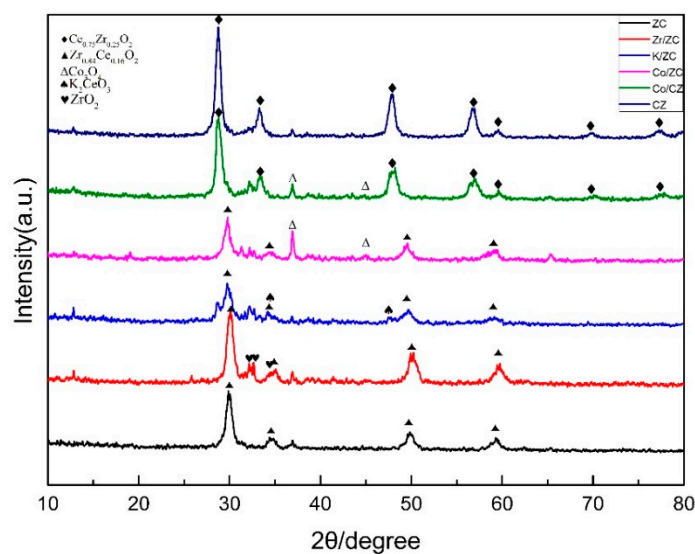


Figure 2. XRD patterns of the catalysis. $\text{Ce}_{0.75}\text{Zr}_{0.25}\text{O}_2$ (CZ), $\text{Zr}_{0.84}\text{Ce}_{0.16}\text{O}_2$ (ZC), 0.8 M of $\text{Zr}(\text{NO}_3)_4 \cdot 5\text{H}_2\text{O}$ was added in $\text{Zr}_{0.84}\text{Ce}_{0.16}\text{O}_2$ (named Zr/ZC), 0.8 M of KNO_3 added in $\text{Zr}_{0.84}\text{Ce}_{0.16}\text{O}_2$ (named K/ZC), 0.8 M of $\text{Co}(\text{NO}_3)_2 \cdot 6\text{H}_2\text{O}$ added in $\text{Zr}_{0.84}\text{Ce}_{0.16}\text{O}_2$ (named Co/ZC), 0.8 M of $\text{Co}(\text{NO}_3)_2 \cdot 6\text{H}_2\text{O}$ added in $\text{Ce}_{0.75}\text{Zr}_{0.25}\text{O}_2$ (named Co/CZ).

2.1.3. Thermogravimetric-Differential Scanning Calorimetry Analysis of Soot

In order to display catalytic action, the thermal analysis of soot was carried out first under simulated automotive exhaust situation (10% oxygen and 90% nitrogen). The TG-DSC curve of soot is shown in Figure 3.

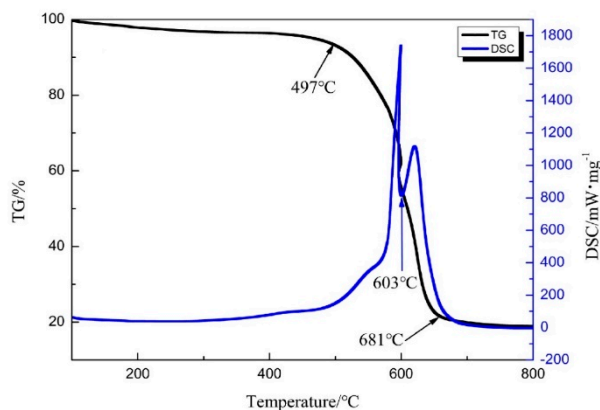


Figure 3. TG-DSC analysis of the soot.

Further, this result was used as a baseline to make comparison with the catalytic sample. The curve reveals that the mass loss occurs in a wide temperature range (497–681 °C), and two endothermic peaks appear simultaneously on the DSC curve. The ignition temperature of soot is 497 °C and the maximum oxidation rate temperature is 603 °C, indicating that all the catalysts involved in the combustion of soot do not require higher temperature to stimulate soot combustion

2.1.4. Thermogravimetric-Differential Scanning Calorimetry Analysis of Samples

So as to simply obtain the ignition temperature (T_i), the maximum oxidation rate temperature (T_o), and the burnout temperature (T_b) of mixture powders (soot + catalyst), the thermal analysis of mixture was carried out first under simulated automotive exhaust situation also. TG-DSC curves of mixture powders (soot + catalyst) are shown in Figure 4 and the T_i , T_o , and burnout temperature are listed in Table 1.

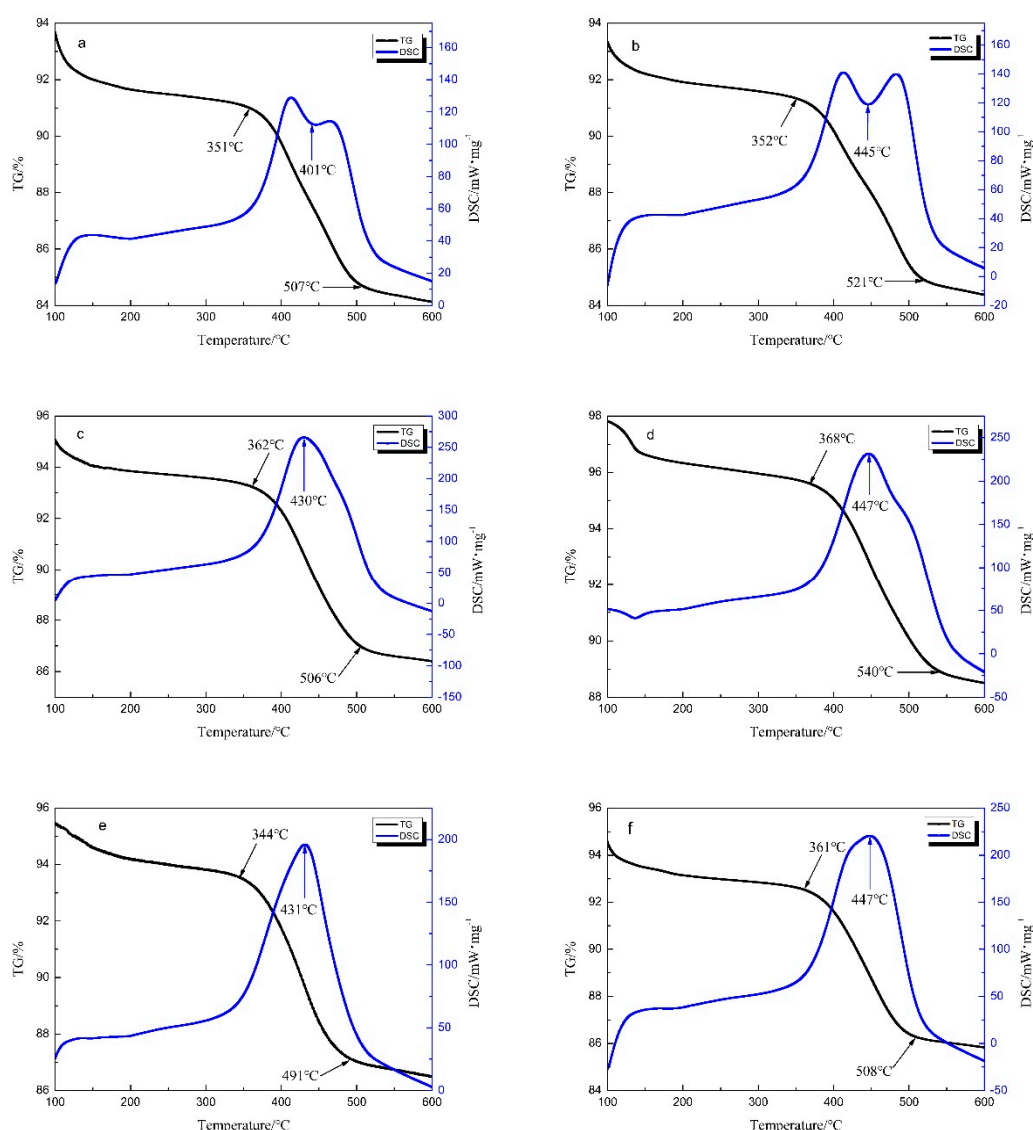


Figure 4. TG-DSC analysis of samples (a)K/ZC + soot, (b) Zr/ZC+ soot, (c) Co/ZC+ soot, (d) ZC + soot, (e)Co/CZ+ soot, (f) CZ+ soot.

It is well known that the $Ce_xZr_{1-x}O_2$ solid solution exhibits higher activity than pure CeO_2 , and $Ce_{0.69}Zr_{0.31}O_2$ (76 wt.% CeO_2) [32] presents the lowest T_{50} value of 455 °C. In order to evaluate catalytic properties, the catalysts and diesel soot (PRINTEX-U) were mechanically mixed for 10 min to obtain

the tight-contact (TC) mode. The results indicated significant decrease in the ignition temperature of soot under the action of these catalysts. In general, the ignition temperature of samples (catalyst + soot) decrease by 100–200 °C under the same testing condition compared to the sample without catalyst. Figure 4d,f exhibit the TG-DSC curves of two different Ce-Zr solid solutions, and results reveal that CZ exhibits better catalytic performance than ZC. Clearly, when Co_3O_4 , ZrO_2 , and K_2CeO_3 phases coexist with $\text{Ce}_x\text{Zr}_{1-x}\text{O}_2$ solid solution, the ignition temperature of soot decreases and the catalytic performance of the catalyst gets improved as presented in Figure 4a–d. Among the catalysts, K/ZC exhibited an excellent effect and the ignition temperature was 351 °C, thus indicating that the oxidation of soot was promoted by increasing the catalyst contact with the high mobility alkali metals [15–19]. Figure 4e–f present the different between Cobalt-doped ZC (Co/CZ) and CZ. The Cobalt-doped ZC reduces the ignition temperature of the soot particles by 153 °C, and 17 °C lower compares to cat-CZ. This result is possibly attributed to the synergistic effect between Co_3O_4 and $\text{Ce}_x\text{Zr}_{1-x}\text{O}_2$ species. The distribution of Co influence the $\text{Ce}_x\text{Zr}_{1-x}\text{O}_2$ crystallite particle size, the specific surface area, and the catalytic activity [33]. In summary, Ce-Zr solid solutions show good catalytic performance for soot combustion, and the Co/CZ ($\text{Co}_3\text{O}_4/\text{CZ}$) sample exhibits the best catalytic performance.

Table 1. The soot combustion parameters with catalysts (data from TG-DSC).

Samples or Soot	Ratio of Catalyst, Soot	Atmosphere/%	$T_i/^\circ\text{C}$	$T_o/^\circ\text{C}$	$T_b/^\circ\text{C}$
Soot			497	603	681
K/ZC			351	401	507
Zr/ZC			352	445	521
Co/ZC	10:1	10% oxygen & 90% nitrogen	362	430	506
ZC			368	447	540
Co/CZ			344	431	491
CZ			361	447	508

2.1.5. X-ray Photoelectron-Spectroscopy Analysis of Catalysts

XPS analysis was conducted to assess the impact of doping on elemental valence. Figure 5a shows the Ce 3d XPS spectra of cat-K/ZC, cat-CZ, and cat-ZC, which demonstrate the presence of eight components, as reported in several relevant studies [34–41]. The Ce 3d spectrum consists of two series of spin-orbit lines u and v. Figure 5a displays that Ce 3d_{3/2} spin-orbit components of cat-ZC which correspond to u lines include three characteristic peaks labeled as u (901.7 eV), u'' (908.9 eV), and u''' (917.0 eV). Ce 3d_{5/2} spin-orbit components which correspond to the series of v lines contain three peaks labeled as v (883.1 eV), v'' (889.7 eV), and v''' (899.1 eV). These three pairs of peaks are attributed to the characteristic peaks of Ce^{4+} . Moreover, the residual two spectral lines labeled as u' (903.7 eV) and v' (886.5 eV) belong to the Ce^{3+} species. According to Lykaki et al. [42], all these eight characteristic peaks shift to the high binding area in our study, because of the formation of Ce-Zr solid solution due to the addition of Zr to the crystal lattice of CeO_2 . Noteworthy, XPS spectra of cat-CZ are different from those of cat-K/ZC and cat-ZC. Ce 3d_{3/2} spin-orbit components of cat-CZ which correspond to u line include three characteristic peaks labeled as u (902.2 eV), u'' (910.9 eV), and u''' (917.0 eV). Ce 3d_{5/2} spin-orbit components which correspond to the series of v lines contain the three peaks labeled as v (882.0 eV), v'' (889.4 eV), and v''' (899.1 eV). However, the peak for cat-K/ZC shifts 0.8 eV toward the low binding energy direction at u'' (908.9 eV), which is caused by K doping. The atomic ratio of $\text{Ce}^{3+}/\text{Ce}^{4+}$ varies to 0.134 (K/ZC), 0.637 (CZ), 0.578 (ZC) after calculated. For catalyst K/ZC, it is obvious that the addition of K reduces the amount of Ce^{3+} , the decrease in the ratio indicates that the Ce^{4+} species is more than the Ce^{3+} , therefore, there are more oxygen vacancies in the catalyst system. The catalysts show excellent redox properties of Ce^{3+} - Ce^{4+} couple and active oxygen storage capacity, which can exchange oxygen in the gas phase. Since the oxygen vacancies can convert the oxygen in the gas phase into active oxygen, enhanced the oxidative properties of the catalyst. So, the soot particles can be ignited at a lower temperature.

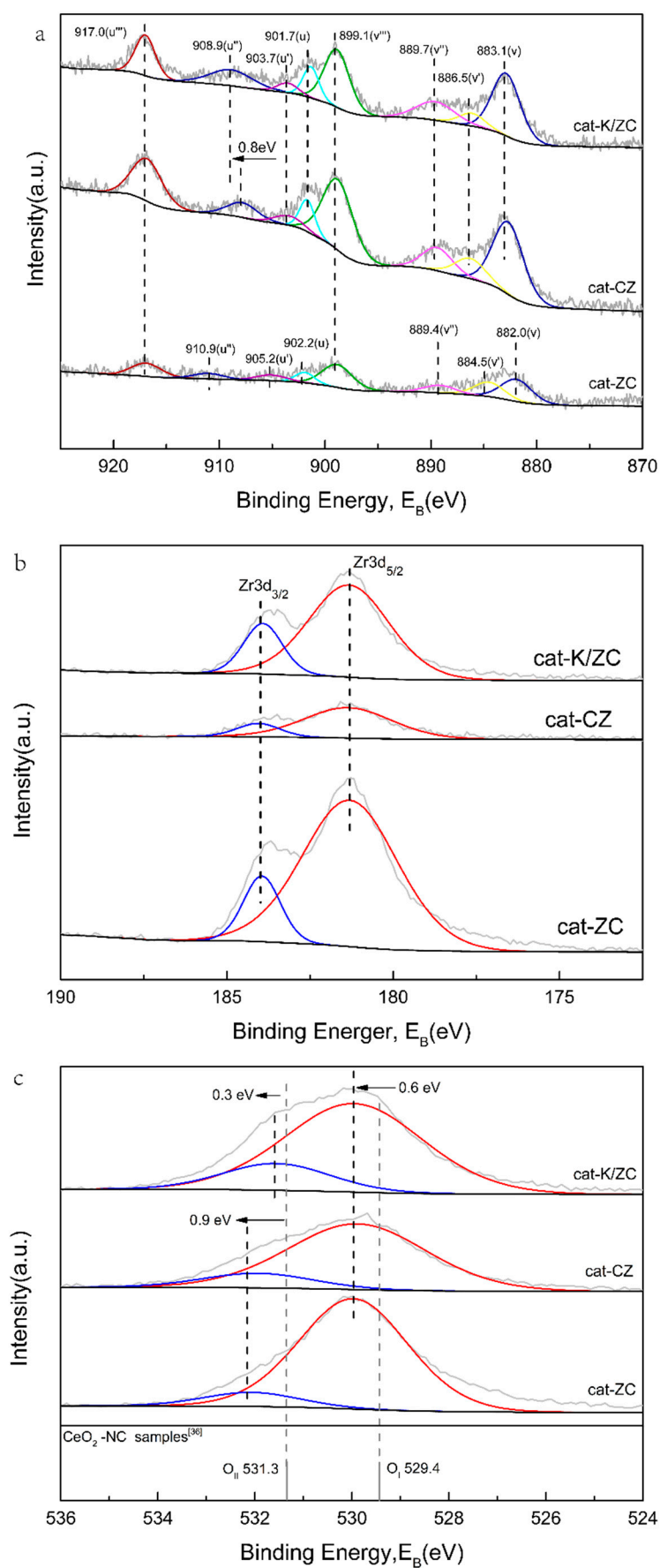


Figure 5. XPS spectra analysis of catalyst K/ZC, ZC and CZ, where (a) Ce 3d, (b) Zr 3d and (c) O 1s.

Figure 5b shows the Zr 3d XPS spectra of cat-K/ZC, cat-CZ, and cat-ZC; compared to the binding energy of Zr 3d_{5/2} and Zr 3d_{3/2} according to *Handbook of the Elements and Native Oxides*, the two characteristic peaks shift 2.8 eV toward the high binding energy. In a word, in Ce-Zr solid solution system, the electron density of outer layer of Ce and Zr increases. The incorporation of isovalent non-reducible elements, Zr⁴⁺ ions, into a ceria lattice has a beneficial influence on the physicochemical and catalytic properties of Ce, improving its thermal stability, oxygen vacancies, and thus can significantly improve the catalytic activity.

The corresponding O 1s XPS spectra are illustrated in Figure 3c, exhibiting the presence of two characteristic peaks in the O 1s spectra of all samples. The primary band (530.0 eV) denoted as O_I represents the lattice oxygen bound to Ce-Zr solid solution system phases, while the shoulder at 532.2 eV (the cat-K/ZC is 531.6 eV) is attributed to chemisorbed oxygen peak (O_{II}) including adsorbed oxygen (O⁻/O₂²⁻), adsorbed water, hydroxyl, and carbonate species. These two characteristic peaks shift to the high binding energy according to open published literature [42]. Zr exhibits a stable state in the catalyst system and can effectively prevent CeO₂ sintering at high temperatures. Ce and Zr form a stable Ce-Zr solid solution, which can enhance the oxygen storage capacity of Ce. Zr⁴⁺ increases the electron density in the system, so the binding energy of O 1s shifts to high energy. Figure 5c clearly reveals that the peak area of adsorbed oxygen of cat-K/ZC is larger than that of cat-ZC and cat-CZ, which indicates more adsorption of oxygen on the surface of cat-K/ZC and easier catalysis of soot particles at a low temperature. Therefore, more soot reacted with adsorbed oxygen, and a higher concentration of CO₂ will be observed at 100–200 °C compared to cat-ZC, which will be discussed in after-mentioned catalytic performance (Section 2.2.). For three samples, the following order, in terms of the O_I / O_{II} ratio, is obtained, K/ZC (5.64) > CZ (4.20) > ZC (4.03), which is perfectly matched to the order of their catalytic performance, as discussed above. These findings along with the TG-DSC results corroborate that the sample with a loose particles, named cat-K/ZC, demonstrate a higher population of loosely bound oxygen species, resulting in improved reducibility. It must be pointed out that the doped-K reduced the electron density of system because the outer electrons number of K less than Ce and Zr, so the binding energy shift to high energy less than 0.6 eV compared to cat-CZ.

2.1.6. Scanning Electron Microscopy and Energy Dispersive Spectroscopy Analysis of Catalyst K/ZC

Figure 6 exhibits the SEM and EDS results of K/ZC after two cycles and five cycles, respectively. And the elemental ratio (wt%) in K/ZC compositions as per the EDS data was listed in Table 2. Morphological characterization by SEM shows that catalyst K/ZC is irregular in shape, which originated from aggregation of nano-particles. K/ZC particles increase the degree of aggregation after five catalytic cycles. Table 2 shows that the catalyst has a stable elemental composition. Even after five cycles of testing, the elemental content of the catalyst still keeps good stability.

Table 2. Elemental ratio (wt%) in K/ZC (second cycles and five cycles) compositions as per the EDS data.

Samples	O K	K K	Ce L	Zr L
K/ZC (two cycles)	35.70 ± 0.87	24.33 ± 3.23	20.82 ± 0.82	19.15 ± 2.47
K/ZC (five cycles)	36.72 ± 1.46	25.79 ± 0.06	20.34 ± 1.19	17.15 ± 1.54

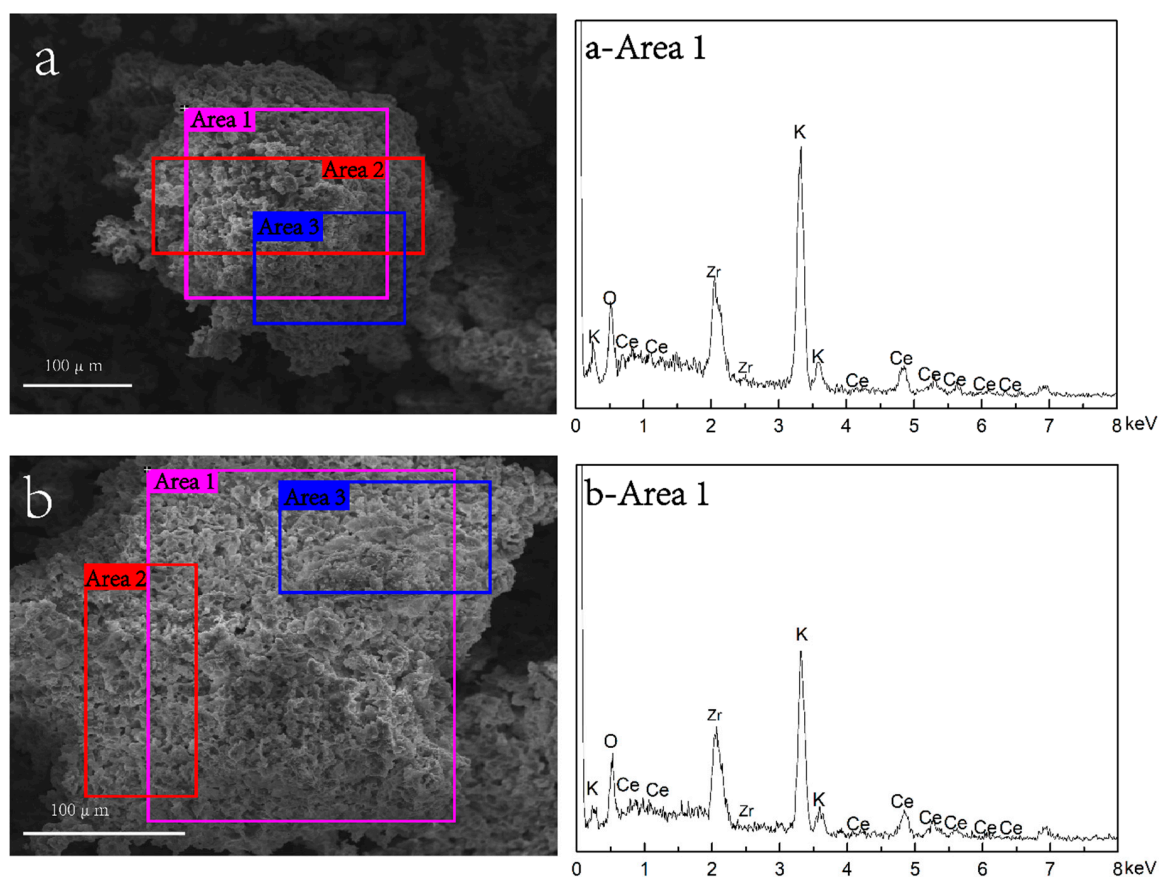


Figure 6. SEM and EDS of catalyst K/ZC after (a) second catalytic cycle, (a-Area 1) EDS of second catalytic cycle in Area 1, (b) five catalytic cycle, (b-Area 1) EDS of five catalytic cycle in Area 1.

2.2. Analysis of Catalytic Performance

Figure 7 shows catalytic oxidation of soot in simulated diesel exhaust. Catalyst K/ZC was selected to test catalytic activity at different oxygen concentrations. Compared to literature results, this simulated diesel exhaust condition was selected to be similar to DOCs (Diesel Oxidation Catalyst) test condition. Comparative analysis of Figure 7a-1 and Figure 7a-2 indicates that very low amount of CO_2 is detected in the 100–200 °C temperature range, which comes from the adsorbed oxygen (O_{ads}) on the catalyst surface. Similarly, it can be seen in the TG-DSC pictures (Figure 4) that these catalysts also has a small amount of weight loss, meaning a little soot was burned at 100–200 °C, this value of weight loss is 1%–2%. As can be seen from Figure 7b-1, the amount of CO_2 released by the catalyst K/ZC at 100–200 °C is significantly more than catalyst CZ and catalyst ZC, which is consistent with the results obtained in Figure 5c. This result prove that there is more adsorption of oxygen on the surface of cat-K/ZC and can easier catalyze more soot particles at a low temperature, just as seen in Figure 5c, the peak area of adsorbed oxygen (O_{II}) of cat-K/ZC is larger than that of cat-ZC and cat-CZ. In contrast, a large amount of CO_2 is detected in the temperature range from 300–400 °C, which is ascribed to the reaction of lattice oxygen (O_{lat}) in the catalysts with soot, thus releasing CO_2 . Concentration of CO_2 exhibits relationship with the oxygen concentration, i.e., the sum of the CO_2 concentration and the O_2 concentration is a constant value related to the incoming O_2 concentration. This indicates that the CO_2 concentration curve and the O_2 concentration curve are complementary.

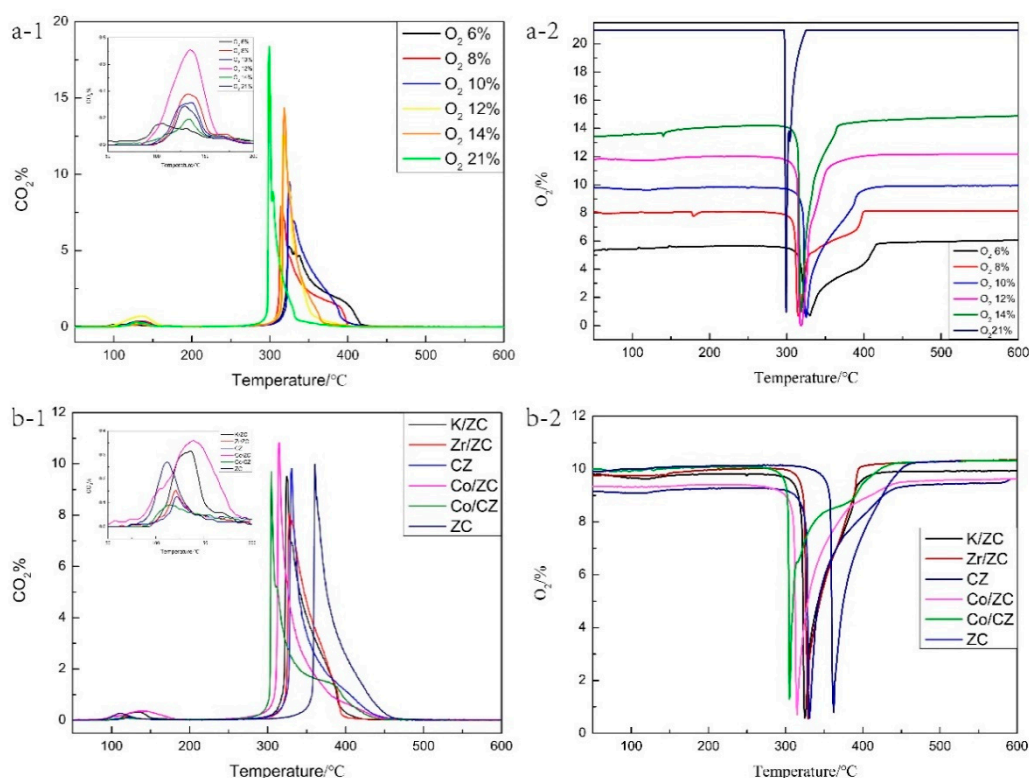


Figure 7. Soot combustion temperature test of (a-1) CO₂ % vs. temperature in different oxygen concentration, (a-2) O₂ % vs. temperature in different oxygen concentration, (b-1) CO₂ % vs. temperature with different catalysts, (b-2) O₂ % vs. temperature with different catalysts. Catalyst used in (a-1) and (a-2), K/ZC.

The CO₂ concentration curves are close to trapezoidal shape, while the oxygen concentration is 6%, 8%, 10%, 12%, and 14%. This is a hysteresis effect which indicates that the soot particles could not burn out in an insufficient oxygen situation. Irrespective of the catalyst tested under test conditions with a same oxygen concentration of 10%, the highest concentration of CO₂ was almost the same, which confirms that the oxygen concentration limits the highest concentration of CO₂. Figure 7b-1 demonstrates that the ignition temperatures of the diesel soot mixed with catalysts decrease apparently, the catalyst Co/ZC shows the lowest ignition temperature (294.2 °C), and the catalyst ZC exhibits the highest ignition temperature (338.5 °C). The curves for CO₂ concentration in case of Co/CZ present a trapezoidal shape, and that for catalyst ZC with the highest ignition temperature is triangular shape. The soot is rapidly oxidized and burned to CO₂ which removes most of the lattice oxygen of the catalyst. As the oxygen is continuously ventilated and the temperature increases, the catalyst is reactivated and continues to catalyze and oxidize the remaining soot. At higher temperatures, the catalyst can simultaneously catalyze the soot and reactivate with the oxygen. This process occurs almost simultaneously, thus the curve shows a triangular shape.

The soot combustion parameters (O₂ concentration, ignition temperature, maximum oxidation rate temperature, etc.) are listed in Table 3. In the simulation exhaust condition (10% O₂), catalyst Co/CZ acquires the lowest ignition temperature (294.2 °C) and catalyst Zr/ZC shows the lowest burnout temperature (403.3 °C). In a word, the incoming O₂ concentration has important influence on ignition temperature and burnout temperature. Jing X et al. studied spinel-type Pd_xCo_{3-x}O₄ binary active sites on 3D ordered meso-macroporous Ce-Zr-O₂ for catalytic soot oxidation. Its T₁₀ value is 313°C [29], higher than the catalyst Co/CZ. Furthermore, catalyst doping with Pt is more expensive too.

Table 3. The soot combustion parameters with catalysts (data from test platform).

Catalyst X	O ₂ /%	The Ignition Temperature/°C	The Temperature of the Max Oxidation Rate/°C	Maximum CO ₂ Concentration/%	Burnout Temperature (CO ₂ ≤ 0.10%)/°C
K/ZC	6	309.0	324	5.29	425.0
	8	301.1	315	7.84	401.7
	10	307.5	324	9.51	416.7
	12	301.1	317	12.67	400.0
	14	301.6	318	14.35	395.0
	21(air)	289.3	299	18.38	379.2
Zr/ZC	10	308.0	327	9.57	403.3
CZ	10	309.8	330	9.82	454.2
Co/ZC	10	295.8	315	10.83	446.7
Co/CZ	10	294.2	304	9.70	438.3
ZC	10	338.5	360	9.99	462.5

Compared to other researchers' studies, catalyst Co/CZ and Co/ZC have a better catalytic performance. We list the ignition temperature (T_i) (or temperature at 10% of soot conversion (T_{10})) and the temperature of the max oxidation rate (T_o) (or temperature at 50% of soot conversion (T_{50})) of these catalysts in Table 4. Compared to these data from Table 4, Pt [43], Au [44], and Cu [45] doped in a catalyst all have an excellent performance. Among them, Au-doped catalyst has the best effect, but the high cost limits its widely applications. The cobalt-doped Ce-Zr solid solution catalysts have better catalytic effect than other catalysts and has great application prospects because of highly efficient and economical.

Table 4. The soot combustion parameters compared to other catalysts.

Catalyst X	Ratio of Catalyst, Soot	Atmosphere	Flow Rate /mL·min ⁻¹	T_i or T_{10} /°C	T_o or T_{50} /°C
Co/ZC	10:1	10% O ₂ & 90% N ₂	100	295.8	315
Co/CZ				294.2	304
Pt@CeO _{2-δ} /Ce _{0.8} Zr _{0.2} O ₂ [43]		5% O ₂ balanced with Ar	50	316	408
Pt@CeO _{2-δ} /Ce _{0.2} Zr _{0.8} O ₂ [43]				358	440
Ce _{0.8} Zr _{0.2} O ₂ (particles) [44]		5% O ₂ and 0.2% NO in Ar	50	381	449
Ce _{0.8} Zr _{0.2} O ₂ (3DOM) [44]				328	394
Au/Ce _{0.8} Zr _{0.2} O ₂ (3DOM) [44]				232	365
Cu _{0.1} Ce _{0.45} Zr _{0.45} O _{2-δ} [45]				382	494
Cu _{0.5} Ce _{0.25} Zr _{0.25} O _{2-δ} [45]		800ppm NO, 6.5 vol% O ₂ balanced with N ₂	500	368	472
Cu _{0.9} Ce _{0.05} Zr _{0.05} O _{2-δ} [45]				284	468

It's reported that alkali metal doping may cause catalyst poisoning and deactivation [46–48]. Therefore, it's necessary to evaluate the cyclic stability of the catalyst which was doped with alkali metal. Thus, K/ZC was selected as a representative specimen to carry out the cyclic stability experiment in this study. Concentration of gases was measured directly through the testing platform to confirm some parameters of soot catalytic combustion, and the corresponding curves are shown in Figure 8. In the first catalytic cycle, T_i (307.5 °C) and T_o (324.2 °C) are different from others cycles. A reasonable explanation is that catalyst K/ZC maintains active framework via the sol-gel preparation and these active sites can accelerate catalytic combustion at lower temperature. However, the active site gets destroyed after the first soot combustion process and the catalyst acquires the stable state, thus T_i and T_o (from the second cycle to the fifth cycle) have almost the same value. It can be seen from the SEM (Figure 6) that the microstructure of the catalyst K/ZC is very stable after two cycles and five cycles. Moreover, the content of each element of the catalyst keeps a stable value, from the results of EDS. Through this sustainable repeated experiment, it was confirmed that the K/ZC catalyst possesses good structural stability and catalytic performance stability, which has an important application in soot combustion field.

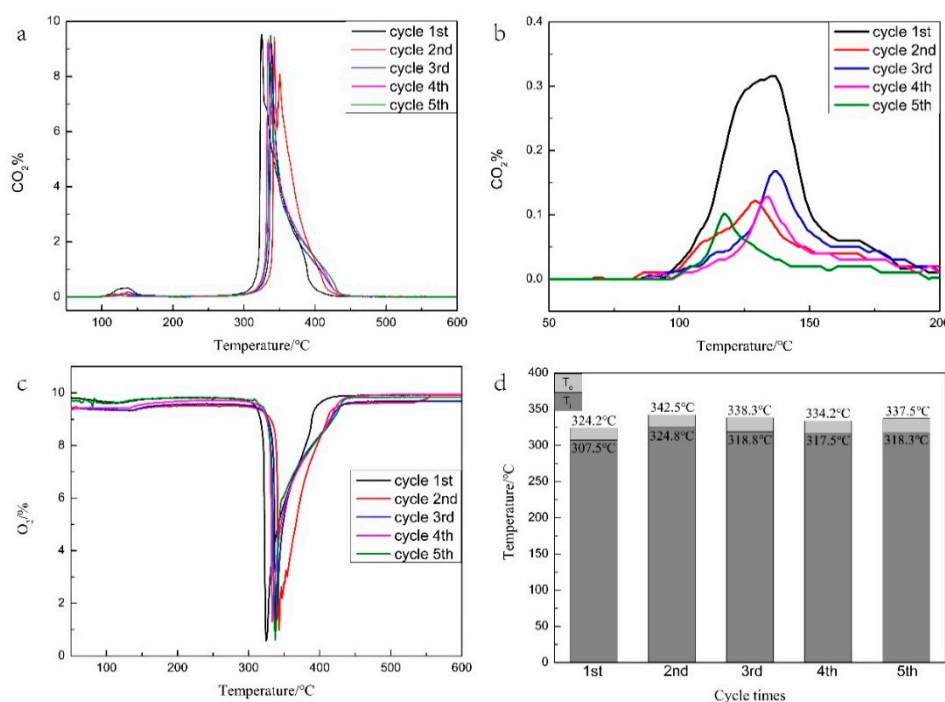


Figure 8. Catalyst K/ZC (a,b) CO₂ % vs. temperature (c) O₂ % vs. temperature (d) the ignition temperature (T_i) and the temperature of the maximum oxidation rate (T_o) vs. catalytic cycle times.

In all XRD showed that the catalysts prepared by the sol-gel method have good crystallinity. SEM characterization results showed that many small catalyst particles are deposited on the Co-doped catalyst, which get a closer contact with the soot. And the soot was been ignited in a lower temperature, which was demonstrated by platform testing. The TG-DSC analysis and platform testing showed that the Ce-Zr solid solution catalyst can effectively reduce the ignition temperature and the temperature of the max oxidation rate of soot particles. Doping different metals (K, Zr, Co) in the Ce-Zr solid solution system can make the ignition temperature of soot particles reduced more. EDS exhibited that the elemental mass percentage of catalyst kept a stable value after two cycles and five cycles. Even after five cycles of experiments, the catalyst still had a stable structure showing good stability, which is along the results from the platform test.

The present findings can be rationalized based on Mars–van Krevelen redox-type mechanism, well documented in literature reports [49–53], and the catalyst reaction process is shown in Figure 9. When the catalyst is in contact with the soot, the exhaust gas provides a high temperature environment so that the soot can take away the lattice oxygen in the catalyst. Several reaction steps take place as follows,

- (i) The lattice oxygen in catalyst reacts very easily with soot towards the formation of active species.
- (ii) The lattice oxygen in the catalyst reacts with active species to form CO₂
- (iii) Oxygen is supplied to the catalyst during continuous aeration, filling the oxygen deficiency in the catalyst, and thus the catalyst is regenerated.

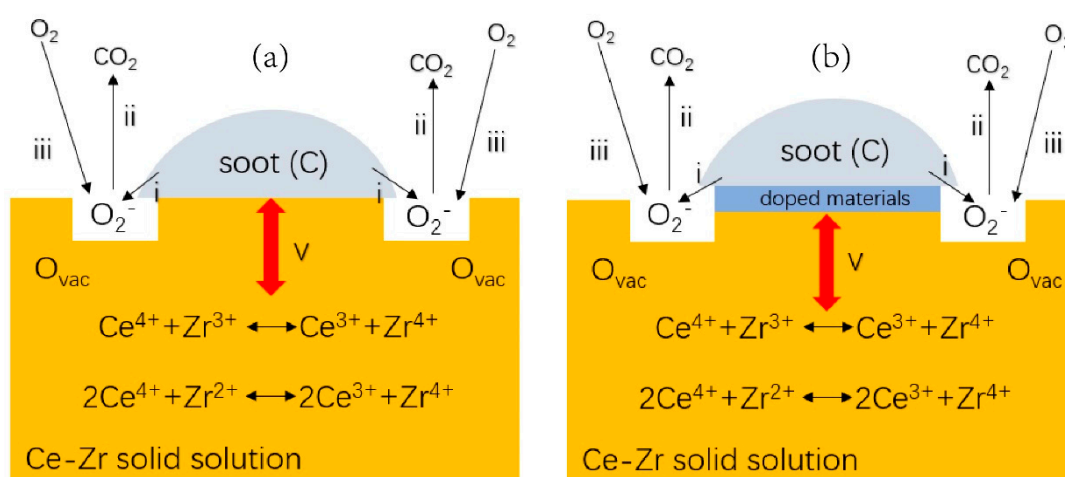


Figure 9. Catalyst reaction process (a) Ce-Zr solid solution, (b) Ce-Zr solid solution doped with K, Co or Zr.

This reaction mechanism can be used to explain why the CO₂ concentration curve of Co/CZ catalyst presents a trapezoidal shape and that of ZC catalyst presents a triangular shape as presented in Figure 8b. When the temperature reaches the temperature of the maximum oxidation rate, the soot is rapidly oxidized and burned to CO₂ which depletes most of the lattice oxygen of catalysts. As the oxygen is continuously ventilated and the temperature increases, catalysts reactivate and continue to catalyze and oxidize the remaining soot. Further, the soot burns catalytically with the oxygen, thus it shows a triangular shape as presented in Figure 8b. The catalyst is cycled back and forth to complete the regeneration process. The doped (K, Co, Zr) catalyst shows larger oxygen vacancy, so that it can catalyze the soot at lower temperature.

3. Materials and Methods

3.1. Materials Preparation

A series of catalysts was prepared by the citric acid sol-gel method using metal nitrate precursors. Cobalt nitrate hexahydrate (Co(NO₃)₂·6H₂O, AR, Kermel Chemical Reagent Co. Tianjin, China), cerium nitrate hexahydrate (Ce(NO₃)₃·6H₂O, AR, Shanpu Chemical Reagent Co. Shanghai, state abbrev if USA, China), zirconium nitrate pentahydrate (Zr(NO₃)₄·5H₂O, AR, Kermel Chemical Reagent Co.), potassium nitrate (KNO₃, AR, Hongyan chemical reagent Co.) and citric acid (C₆H₈O₇, AR, Huada Chemical Reagent Co. Changzhou, state abbrev if USA, China) were used as raw materials in the present study. Firstly, Ce(NO₃)₃·6H₂O (3.256 g, 7.5 mmol) was dissolved in 20 mL deionized water, and a solution of Zr(NO₃)₄·5H₂O (1.073 g, 2.5 mmol) in 20 mL was added. The mixture was stirred for 20 min at room temperature, and then mixed with citric acid solution which was equal to the total moles of Ce(NO₃)₃·6H₂O and Zr(NO₃)₄·5H₂O. The resulting amaranthine solution was stirred continuously at 85 °C for 1.5 h holding time, and the mixture solution gradually transformed into a viscous gel. After that, the wet gel was dried at 110 °C in the furnace for 48 h, and the loose purple powder was obtained after grinding treatment. Finally, the powder was heated from room temperature to 600 °C for 5 h sintering in muffle furnace, the sample of Ce_{0.75}Zr_{0.25}O₂ (named CZ) was obtained. According to the similar fabrication processes, Zr_{0.84}Ce_{0.16}O₂ (named ZC) was formed controlling Zr/Ce molar ratio to be 21,4, zirconium-riched Zr_{0.84}Ce_{0.16}O₂ (named Zr/ZC) was prepared controlling Zr/Ce molar ratio to be 21,2, potassium-doped Zr_{0.84}Ce_{0.16}O₂ (named K/ZC) was prepared controlling K, Zr, Ce to be 21,4,4, cobalt-doped Zr_{0.84}Ce_{0.16}O₂ (named Co/ZC) was formed controlling Co, Zr, Ce to be 21,4,4, and cobalt-doped Ce_{0.75}Zr_{0.25}O₂ (named Co/CZ) was fabricated controlling Co, Ce, Zr to be 3,3,1.

3.2. Characterization

X-ray diffraction (XRD) patterns of the samples were obtained with an AXS D8 Advance diffractometer (Bruker, Germany) with Cu K α radiation (0.154 nm) operating at 40 kV and 30 mA. The XRD patterns were recorded in the 2 $^{\circ}$ range of 10 $^{\circ}$ –80 $^{\circ}$ with a scanning rate of 10 $^{\circ}$ /min. The morphology of the samples were observed by field-emission scanning electron microscopy (S-4800, Hitachi, Tokyo, Japan) with a 10 kV operating voltage. The energy dispersive spectrometer (EDS) of the samples were observed by field-emission scanning electron microscopy (Quanta 600F, FEI, Hillsboro, OR, USA) attached to an a EDS (INCA-350, Oxford Instruments, Oxfordshire, UK). Thermal analysis was performed in a simultaneous thermogravimetry and differential scanning calorimetry (TG-DSC) (STA 449F5, Netzsch, Selb, Germany). The thermal analysis of samples was carried out under simulated automotive exhaust situation (10% oxygen and 90% nitrogen, 100 mL/min) (from 50 $^{\circ}$ C to 600 $^{\circ}$ C, 10 $^{\circ}$ C/min). The X-ray photoelectron spectroscopy (XPS) was recorded on a PHI quantera II instrument (ULVAC, Japan) under ultra-high vacuum using a monochromated Al K α source (1486.6 eV) at 42.1 W. The measurements were performed at 20 eV pass energy, 0.1 eV step and 0.15 min dwelling time.

3.3. Catalytic Properties

Schematic illustration of soot combustion test platform is shown in Figure 10. A mass flow controller is used to control the experimental atmosphere. A tubular muffle furnace is used for programmed heating of samples. Gases concentration data through exhaust gas analyser record by computer. The catalysts and diesel soot were mechanically mixed in tight-contact (TC) and then the mixture was placed into tubular muffle furnace. First, using N $_2$ to remove the exhaust gas, and the catalyst was mixed with carbon black particles (PRINTEX-U) in 10:1 ratio. Then, the mixture (0.55 g) was accurately weighed and placed in a quartz tube. Subsequently, input mass flow of gases was controlled to simulate the diesel engine exhaust and gases concentration data through exhaust gas analyser and muffle furnace heating temperature were recorded.

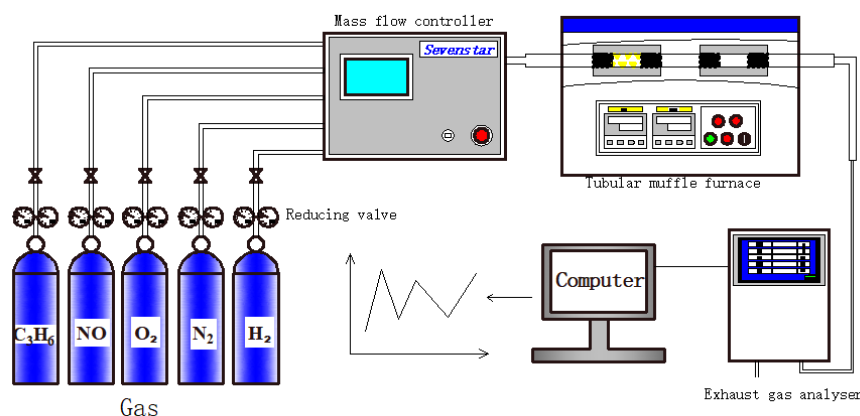


Figure 10. Soot combustion test platform.

In order to evaluate the cyclic stability of the catalyst, K/ZC was selected as a specimen to carry out cyclic stability experiment in this study. After different cycle times, catalysts were characterized by SEM and EDS for research on microstructural stability and composition stability.

4. Conclusions

Remarkable catalytic performance, thermostability, and repetition stability of catalysts (K/Zr $_{0.84}$ Ce $_{0.16}$ O $_2$, Zr/Zr $_{0.84}$ Ce $_{0.16}$ O $_2$, Co/Zr $_{0.84}$ Ce $_{0.16}$ O $_2$, Zr $_{0.84}$ Ce $_{0.16}$ O $_2$, Co/Ce $_{0.75}$ Zr $_{0.25}$ O $_2$, and Ce $_{0.75}$ Zr $_{0.25}$ O $_2$) prepared by sol–gel method make it possible to use these catalysts in diesel emission control. In the Ce–Zr solid solution system, Zr increase the oxygen storage capacity of Ce and prevent cerium oxide from sintering at high temperatures. The incorporation of isovalent non-reducible

elements, Zr^{4+} ions, into a ceria lattice has a beneficial influence on the physicochemical and catalytic properties of Ce, improving its thermal stability, oxygen vacancies, and thus can significantly improve the catalytic activity. By doping different elements (Co, Zr, and K), the ignition temperature and the temperature of the max oxidation rate of the soot particles can be significantly reduced. The catalysts show excellent redox properties of Ce^{3+} - Ce^{4+} couple and active oxygen storage capacity, which can exchange oxygen in the gas phase. Compared to catalyst CZ and catalyst ZC, the atomic ratio of Ce^{3+}/Ce^{4+} of catalyst K/ZC is 0.13, it is obvious that the addition of K reduces the amount of Ce^{3+} species and there are more oxygen vacancies in the catalyst system, allowing it to ignite the soot at a lower temperature. SEM images show that many small particles are deposited on the cobalt-doped catalyst (Co/CZ and Co/ZC), which can lead to a better contact of the catalyst with the soot, resulting a lower ignition temperature. The catalytic performance studies revealed that the Co/Ce_{0.75}Zr_{0.25}O₂ catalyst showed the lowest ignition temperature. The results revealed that some soot particles could react with adsorbed oxygen, and other part of diesel soot reacted with lattice oxygen. The activity of these catalysts is attributed to synergistic effect arising from the combination of K/Co/Zr and Ce-Zr solid solution, which leads to the decrease in ignition temperature to 294 °C (data from the test platform). Furthermore, the reaction mechanism for the oxidation reactions of soot was proposed, combination of K/Co/Zr with Ce-Zr solid solution reduces the binding energy of Ce-Zr solid solution, which is conducive in providing more active sites to release the active oxygen (O_2^-) or lattice oxygen (O^{2-}). It is thus proved that the K/ZC catalyst possesses good structural stability and catalytic performance stability as indicated by the catalyst stability experiment, and thus shows potential application prospects for effective removal of diesel soot. In a word, these high efficient, long life period and economical catalyst make it possible to use for combustion of diesel soot.

Author Contributions: Formal analysis, P.W.; writing—original draft preparation, C.A.; Investigation, Y.Z.; writing—review and editing, W.W.; funding acquisition, W.W.

Funding: This research was funded by National Natural Science Foundation of China, grant number 51678059. The Key Research and Development Program of Shaanxi Province, grant number 2019GY-179. The Fundamental Research Funds for the Central Universities, grant number 300102298202. The Open Foundation of the Laboratory of Degraded and Unused Land Consolidation Engineering, the Ministry of Land Resources, grant number SXDJ2017-1 and the Open Foundation of Key Laboratory of Shaanxi Provincial Land Rehabilitation, grant number 2018-JC10.

Acknowledgments: This work was supported by National Natural Science Foundation of China. Thanks to Pan Wang for providing support for the test platform (School of Automotive and Traffic Engineering, Jiangsu University).

Conflicts of Interest: The authors declare no conflict of interest.

References

1. Zhu, Q.; Sun, Y.; Na, F.; Wei, J.; Xu, S.; Li, Y.; Guo, F. Fabrication of CdS/titanium-oxo-cluster nanocomposites based on a Ti32 framework with enhanced photocatalytic activity for tetracycline hydrochloride degradation under visible light. *Appl. Catal. B* **2019**, *254*, 541–550. [[CrossRef](#)]
2. Wang, H.; Liang, Y.; Liu, L.; Hu, J.; Cui, W. Highly ordered TiO₂ nanotube arrays wrapped with g-C₃N₄ nanoparticles for efficient charge separation and increased photoelectrocatalytic degradation of phenol. *J. Hazard. Mater.* **2018**, *344*, 369–380. [[CrossRef](#)] [[PubMed](#)]
3. Rao, L.; Liu, S.; Wang, L.; Ma, C.; Wu, J.; An, L.; Hu, X. N-doped porous carbons from low-temperature and single-step sodium amide activation of carbonized water chestnut shell with excellent CO₂ capture performance. *Chem. Eng. J.* **2019**, *359*, 428–435. [[CrossRef](#)]
4. Li, Y.; Zhang, N.; Xu, S.; Zhu, Q.; Hu, J. The influence of temperature on the phase behavior of ionic liquid aqueous two-phase systems. *J. Dispersion Sci. Technol.* **2019**, *40*, 874–883. [[CrossRef](#)]
5. Tuler, F.; Banus, E.D.; Zanuttini, M.; Miró, E.; Milt, V. Ceramic papers as flexible structures for the development of novel diesel soot combustion catalysts. *Chem. Eng. J.* **2014**, *246*, 287–298. [[CrossRef](#)]
6. Partanen, A.-I.; Landry, J.-S.; Matthews, H.D. Climate and health implications of future aerosol emission scenarios. *Environ. Res. Lett.* **2018**, *13*, 024028. [[CrossRef](#)]

7. Voiland, A. Aerosols, Tiny Particles, Big Impact. Available online: <https://earthobservatory.nasa.gov/features/Aerosols> (accessed on 2 November 2010).
8. Bueno-López, A. Diesel soot combustion ceria catalysts. *Appl. Catal. B* **2014**, *146*, 1–11. [[CrossRef](#)]
9. Cao, Q.; Rui, G.; Liang, Y. Study on PM_{2.5} pollution and the mortality due to lung cancer in China based on geographic weighted regression model. *BMC Public Health* **2018**, *18*, 925. [[CrossRef](#)]
10. Kittelson, D.; Watts, W.; Johnson, J. On-road and laboratory evaluation of combustion aerosols part 1, summary of diesel engine results. *Aerosol Sci.* **2006**, *37*, 913–930. [[CrossRef](#)]
11. Piumetti, M.; Andana, T.; Bensaid, S.; Fino, D.; Russo, N.; Pirone, R. Ceria-based nanomaterials as catalysts for CO oxidation and soot combustion, Effect of Zr-Pr doping and structural properties on the catalytic activity. *AIChE J.* **2016**, *63*, 216–225. [[CrossRef](#)]
12. Zhu, H.; Xu, J.; Yichuan, Y.; Wang, Z.; Gao, Y.; Liu, W.; Yin, H. Catalytic oxidation of soot on mesoporous ceria-based mixed oxides with cetyltrimethyl ammonium bromide (CTAB)-assisted synthesis. *J. Colloid Interface Sci.* **2017**, *508*, 1–13. [[CrossRef](#)] [[PubMed](#)]
13. Rout, K.R.; Fenes, E.; Baidoo, M.F.; Abdollahi, R.; Fuglerud, T.; Chen, D. Highly Active and Stable CeO₂-Promoted CuCl₂/Al₂O₃ Oxychlorination Catalysts Developed by Rational Design Using a Rate Diagram of the Catalytic Cycle. *ACS Catal.* **2016**, *6*, 7030–7039. [[CrossRef](#)]
14. Yang, C.; Yu, X.; Heißler, S.; Nefedov, A.; Colussi, S.; Llorca, J.; Trovarelli, A.; Wang, Y. Surface Faceting and Reconstruction of Ceria Nanoparticles. *Angew. Chem. Int. Ed.* **2017**, *56*, 375–379. [[CrossRef](#)] [[PubMed](#)]
15. Krishna, K.; Bueno-López, A.; Makkee, M.; Moulijn, J.A. Potential rare earth modified CeO₂ catalysts for soot oxidation, I. Characterisation and catalytic activity with O₂. *Appl. Catal. B* **2007**, *75*, 189–200. [[CrossRef](#)]
16. Castoldi, L.; Matarrese, R.; Lietti, L.; Forzatti, P. Intrinsic reactivity of alkaline and alkaline-earth metal oxide catalysts for oxidation of soot. *Appl. Catal. B* **2009**, *90*, 278–285. [[CrossRef](#)]
17. Eversfield, P.; Liu, W.; Klemm, E. Effect of Potassium on the Physiochemical and Catalytic Characteristics of V₂O₅/TiO₂ Catalysts in o-Xylene Partial Oxidation to Phthalic Anhydride. *Catal. Lett.* **2017**, *147*, 785–791. [[CrossRef](#)]
18. Weng, D.; Li, J.; Wu, X.; Si, Z. Modification of CeO₂-ZrO₂ catalyst by potassium for NO_x-assisted soot oxidation. *J. Environ. Sci.* **2011**, *23*, 145–150. [[CrossRef](#)]
19. Lu, C.; Liu, T.; Shi, Q.; Li, Q.; Xin, Y.; Zheng, L.; Zhang, Z. Plausibility of potassium ion-exchanged ZSM-5 as soot combustion catalysts. *Sci. Rep.* **2017**, *7*, 3300. [[CrossRef](#)]
20. Lin, F.; Wu, X.; Weng, D. Effect of barium loading on CuO_x-CeO₂ catalysts, NO_x storage capacity, NO oxidation ability and soot oxidation activity. *Catal. Today* **2011**, *175*, 124–132. [[CrossRef](#)]
21. Aneggi, E.; de Leitenburg, C.; Dolcetti, G.; Trovarelli, A. Diesel soot combustion activity of ceria promoted with alkali metals. *Catal. Today* **2008**, *136*, 3–10. [[CrossRef](#)]
22. Weng, D.; Li, J.; Wu, X.; Si, Z. NO_x-assisted soot oxidation over K/CuCe catalyst. *J. Rare Earth* **2010**, *28*, 542–546. [[CrossRef](#)]
23. Shan, W.; Yang, L.; Ma, N.; Yang, J. Catalytic Activity and Stability of K/CeO₂ Catalysts for Diesel Soot Oxidation. *Chin. J. Catal.* **2012**, *33*, 970–976. [[CrossRef](#)]
24. Aneggi, E.; Leitenburg, C.D.; Trovarelli, A. On the role of lattice/surface oxygen in ceria-zirconia catalysts for diesel soot combustion. *Catal. Today* **2012**, *181*, 108–115. [[CrossRef](#)]
25. Atribak, I.; Bueno-López, A.; Garcia-Garcia, A. Combined removal of diesel soot particulates and NO_x over CeO₂-ZrO₂ mixed oxides. *J. Catal.* **2008**, *259*, 123–132. [[CrossRef](#)]
26. Atribak, I.; Azambre, B.; Bueno-Lopez, A.; Garcia-Garcia, A. NO_x Adsorption/Desorption Processes Over Ce_{0.76}Zr_{0.24}O₂ and Their Influence on DeSoot Activity, Effect of the Catalyst Calcination Temperature. *Top. Catal.* **2009**, *52*, 2092–2096. [[CrossRef](#)]
27. Atribak, I.; Azambre, B.; López, A.B.; García-García, A. Effect of NO_x adsorption/desorption over ceria-zirconia catalysts on the catalytic combustion of model soot. *Appl. Catal. B* **2009**, *92*, 126–137. [[CrossRef](#)]
28. Atribak, I.; Bueno-López, A.; García-García, A.; Azambre, B. Contributions of surface and bulk heterogeneities to the NO oxidation activities of ceria-zirconia catalysts with composition Ce_{0.76}Zr_{0.24}O₂ prepared by different methods. *Phys. Chem. Chem. Phys.* **2010**, *12*, 13770–13779. [[CrossRef](#)]
29. Xiong, J.; Wu, Q.; Mei, X.; Liu, J.; Wei, Y.; Zhao, Z.; Wu, D.; Li, J. Fabrication of Spinel-Type Pd_xCo_{3-x}O₄ Binary Active Sites on 3D Ordered Meso-macroporous Ce-Zr-O₂ with Enhanced Activity for Catalytic Soot Oxidation. *ACS Catal.* **2018**, *8*, 7915–7930. [[CrossRef](#)]

30. Azambre, B.; Collura, S.; Darcy, P.; Trichard, J.M.; Da Costa, P.; García-García, A.; Bueno-López, A. Effects of a Pt/Ce_{0.68}Zr_{0.32}O₂ catalyst and NO₂ on the kinetics of diesel soot oxidation from thermogravimetric analyses. *Fuel Process. Technol.* **2011**, *92*, 363–371. [[CrossRef](#)]
31. Liu, S.; Wu, X.; Lin, Y.; Li, M.; Weng, D. Active oxygen-assisted NO-NO₂ recycling and decomposition of surface oxygenated species on diesel soot with Pt/Ce_{0.6}Zr_{0.4}O₂ catalyst. *Chin. J. Catal.* **2014**, *35*, 407–415. [[CrossRef](#)]
32. Atribak, I.; Bueno-López, A.; García-García, A. Thermally stable ceria-zirconia catalysts for soot oxidation by O₂. *Catal. Commun.* **2008**, *9*, 250–255. [[CrossRef](#)]
33. Yang, J.; Lukashuk, L.; Akbarzadeh, J.; Stöger-Pollach, M.; Peterlik, H.; Föttinger, K.; Rupprechter, G.; Schubert, U. Different synthesis protocols for Co₃O₄-CeO₂ catalysts-Part 1, influence on the morphology on the nanoscale. *Chem. Eur. J.* **2015**, *21*, 885–892. [[CrossRef](#)] [[PubMed](#)]
34. Cui, Y.; Dai, W.L. Support Morphology and Crystal-plane Effect of Cu/CeO₂ Nano-Material on the Physicochemical and Catalytic Properties for Carbonate Hydrogenation. *Catal. Sci. Technol.* **2016**. [[CrossRef](#)]
35. Zhou, R.; Guo, X. A new insight into the morphology effect of ceria on CuO/CeO₂ catalysts for CO selective oxidation in hydrogen-rich gas. *Catal. Sci. Technol.* **2016**, *6*, 3862–3871.
36. Wang, C.; Cheng, Q.; Wang, X.; Ma, K.; Bai, X.; Tan, S.; Tian, Y.; Ding, T.; Zheng, L.; Zhang, J.; et al. Enhanced catalytic performance for CO preferential oxidation over CuO catalysts supported on highly defective CeO₂ nanocrystals. *Appl. Surf. Sci.* **2017**, *422*, 932–943. [[CrossRef](#)]
37. Konsolakis, M.; Carabineiro, S.A.C.; Marnellos, G.E.; Asad, M.F.; Soares, O.S.G.P.; Pereira, M.F.R.; Órfão, J.J.M.; Figueiredo, J.L. Effect of cobalt loading on the solid state properties and ethyl acetate oxidation performance of cobalt-cerium mixed oxides. *J. Colloid Interface Sci.* **2017**, *496*, 141–149. [[CrossRef](#)] [[PubMed](#)]
38. Carabineiro, S.A.C.; Bastos, S.S.T.; Órfão, J.J.M.; Pereira, M.F.R.; Delgado, J.J.; Figueiredo, J.L. Exotemplated ceria catalysts with gold for CO oxidation. *Appl. Catal. A* **2010**, *381*, 150–160. [[CrossRef](#)]
39. Carabineiro, S.A.C.; Silva, A.M.T.; Dražić, G.; Tavares, P.B.; Figueiredo, J.L. Gold nanoparticles on ceria supports for the oxidation of carbon monoxide. *Catal. Today* **2010**, *154*, 21–30. [[CrossRef](#)]
40. Carabineiro, S.A.C.; Konsolakis, M.; Marnellos, G.E.-N.; Asad, M.F.; Soares, O.S.G.P.; Tavares, P.B.; Pereira, M.F.R.; Órfão, J.J.D.M.; Figueiredo, J.L. Ethyl Acetate Abatement on Copper Catalysts Supported on Ceria Doped with Rare Earth Oxides. *Molecules* **2016**, *21*, 644. [[CrossRef](#)]
41. Konsolakis, M.; Carabineiro, S.A.C.; Marnellos, G.E.; Asad, M.F.; Soares, O.S.G.P.; Pereira, M.F.R.; Órfão, J.J.M.; Figueiredo, J.L. Volatile organic compounds abatement over copper-based catalysts, effect of support. *Inorg. Chim. Acta* **2017**, *455*, 473–482. [[CrossRef](#)]
42. Lykaki, M.; Pachatouridou, E.; Carabineiro, S.A.; Iliopoulou, E.; Andriopoulou, C.; Kallithrakas-Kontos, N.; Boghosian, S.; Konsolakis, M. Ceria Nanoparticles Shape Effects on the Structural Defects and Surface Chemistry, Implications in CO oxidation by Cu/CeO₂ oxides. *Appl. Catal. B* **2018**, *230*, 18–28. [[CrossRef](#)]
43. Wei, Y.; Jiao, J.; Zhang, X.; Jin, B.; Zhao, Z.; Xiong, J.; Li, Y.; Liu, J.; Li, J. Catalysts of self-assembled Pt@CeO_{2-δ}-rich core-shell nanoparticles on 3D ordered macroporous Ce_{1-x}Zr_xO₂ for soot oxidation, nanostructure-dependent catalytic activity. *Nanoscale* **2017**, *9*, 4558–4571. [[CrossRef](#)]
44. Guan, B.; Lin, H.; Zhan, R.; Huang, Z. The catalysts of three-dimensionally ordered macroporous Ce_{1-x}Zr_xO₂-supported gold nanoparticles for soot combustion, The metal-support interaction. *J. Catal.* **2012**, *287*, 13–29.
45. Guan, B.; Lin, H.; Zhan, R.; Huang, Z. Catalytic combustion of soot over Cu, Mn substitution CeZrO_{2-δ}, nanocomposites catalysts prepared by self-propagating high-temperature synthesis method. *Chem. Eng. Sci.* **2018**, *189*, 320–339. [[CrossRef](#)]
46. Xu, B.; Xu, H.; Lin, T.; Cao, Y.; Lan, L.; Li, Y.; Feng, X.; Gong, M.; Chen, Y. Promotional effects of Zr on K⁺-poisoning resistance of CeTiO_x catalyst for selective catalytic reduction of NO_x with NH₃. *Chin. J. Catal.* **2016**, *37*, 1354–1361. [[CrossRef](#)]
47. Wang, H.; Chen, X.; Gao, S.; Wu, Z.; Liu, Y.; Weng, X. Deactivation mechanism of Ce/TiO₂ selective catalytic reduction catalysts by the loading of sodium and calcium salts. *Catal. Sci. Technol.* **2013**, *3*, 715–722. [[CrossRef](#)]
48. Li, M.Y.; Guo, R.T.; Hu, C.X.; Sun, P.; Pan, W.G.; Liu, S.M.; Sun, X.; Liu, S.W.; Liu, J. The enhanced resistance to K deactivation of Ce/TiO₂ catalyst for NH₃-SCR reaction by the modification with P. *Appl. Surf. Sci.* **2017**, *436*, 814–822. [[CrossRef](#)]

49. Wang, W.W.; Yu, W.Z.; Du, P.P.; Xu, H.; Jin, Z.; Si, R.; Ma, C.; Shi, S.; Jia, C.J.; Yan, C.H. Crystal Plane Effect of Ceria on Supported Copper Oxide Cluster Catalyst for CO Oxidation, Importance of Metal–Support Interaction. *ACS Catal.* **2017**, *7*, 1313–1329. [[CrossRef](#)]
50. Sun, J.; Zhang, L.; Ge, C.; Tang, C.; Dong, L. Comparative study on the catalytic CO oxidation properties of CuO/CeO₂ catalysts prepared by solid state and wet impregnation. *Chin. J. Catal.* **2014**, *35*, 1347–1358. [[CrossRef](#)]
51. Yao, S.; Mudiyansele, K.; Xu, W.; Johnston-Peck, A.C.; Hanson, J.C.; Wu, T.; Stacchiola, D.; Rodriguez, J.A.; Zhao, H.; Kevin, A.; et al. Unraveling the dynamic nature of a CuO/CeO₂ catalyst for CO oxidation in Operando, A combined study of XANES (Fluorescence) and DRIFTS. *ACS Catal.* **2014**, *4*, 1650–1661. [[CrossRef](#)]
52. Qi, L.; Yu, Q.; Dai, Y.; Tang, C.; Liu, L.; Zhang, H.; Gao, F.; Dong, L.; Chen, Y. Influence of cerium precursors on the structure and reducibility of mesoporous CuO–CeO₂ catalysts for CO oxidation. *Appl. Catal. B* **2012**, *119–120*, 308–320. [[CrossRef](#)]
53. Jia, A.-P.; Jiang, S.-Y.; Lu, J.-Q.; Luo, M.-F. Study of Catalytic Activity at the CuO–CeO₂ Interface for CO Oxidation. *J. Phys. Chem. C* **2010**, *114*, 21605–21610. [[CrossRef](#)]



© 2019 by the authors. Licensee MDPI, Basel, Switzerland. This article is an open access article distributed under the terms and conditions of the Creative Commons Attribution (CC BY) license (<http://creativecommons.org/licenses/by/4.0/>).